



An efficient finite-rate chemistry model for a preconditioned compressible flow solver and its comparison with the flamelet/progress-variable model



Suo Yang¹, Xingjian Wang, Hongfa Huo, Wenting Sun, Vigor Yang*

School of Aerospace Engineering, Georgia Institute of Technology, Atlanta, GA 30332, USA

ARTICLE INFO

Article history:

Received 20 December 2018
Revised 21 August 2019
Accepted 22 August 2019
Available online 4 September 2019

Keywords:

Turbulent combustion
Large eddy simulation
Finite-rate chemistry
Flamelet/progress-variable

ABSTRACT

An efficient finite-rate chemistry (FRC) model is developed for a preconditioned compressible flow solver. The model uses a point-implicit stiff ODE solver and a correlated dynamic adaptive chemistry algorithm. With respect to the conventional FRC model using the double precision variable coefficient stiff ODE solver, the present work achieves an 8.6 times speed-up for chemistry calculation, and 6.4 times for total computation, when using a 20-species kinetics mechanism for methane/air flames. As an example problem, a piloted partially premixed methane/air jet flame (Sandia Flame D), with a relatively low level of local extinction and re-ignition, is considered, and both the new FRC-large eddy simulation (LES) and flamelet/progress-variable (FPV)-LES are conducted. The FRC-LES approach predicts larger time-averaged flame length, and better agrees with the measured value. This is because the instantaneous high-temperature zone for the FPV-LES case is significantly smaller than its FRC-LES counterpart, especially in the downstream region. For spatial distribution of time-averaged statistics, the FPV-LES result agrees with the experimental data better. For conditional statistics in the mixture fraction space, the FRC-LES approach provides significantly better predictions. Near the stoichiometric region, in comparison with experimental data and the FRC-LES results, the FPV-LES approach predicts higher radical generation, but lower CO generation and heat release.

© 2019 The Combustion Institute. Published by Elsevier Inc. All rights reserved.

1. Introduction

High-fidelity simulation of turbulent combustion provides quantitative solutions with minimal empirical constants. Large-eddy simulation (LES) has drawn significant attention in decades, and its predictive capability is continuously improving. In LES, the energy-containing large-eddy motions are resolved with sufficient grid resolution, while motions of scales smaller than the grid sizes, subgrid-scale (SGS) motions, are modeled. Chemical reaction rates are highly nonlinear functions of species concentrations and temperature, which depend strongly on turbulent mixing; at the same time, chemical reactions release heat and subsequently affect species concentrations and temperature, which in turn change the turbulent mixing. Chemical reactions occurring at different time scales may interact with eddies of different length and time scales, further complicating the physiochemical processes.

Turbulence/chemistry interaction is thus considered the most challenging problem in turbulent combustion modeling.

Turbulent combustion models that have been developed for LES can be classified into two major categories: finite-rate chemistry (FRC) models, and reduced-order manifold models. The former category includes the laminar chemistry model [1], the eddy dissipation concept (EDC) model for the turbulence–chemistry interaction coupled with the perfectly-stirred reactor (PSR) model for FRC [2], the partially-stirred reactor (PaSR) model [3], the linear-eddy model (LEM) [4], the Monte Carlo method for Lagrangian filtered probability density function (PDF) transport equations [5], and the thickened flame model (TFM) [6]. The latter category includes the steady laminar flamelet model [7], the Lagrangian flamelet model [8,9], and the flamelet/progress-variable (FPV) model [10].

Among reduced-order manifold models, the steady laminar flamelet model pioneered by Peters [7] offers the advantages of easy implementation and low computational cost. There are, however, limitations associated with this model. First, the mixture fraction does not really carry information about chemical states. The model uses the filtered dissipation rate of the mixture fraction as an additional parameter to account for the flame stretching effect. The dissipation rate, however, does not provide a unique mapping

* Corresponding author.

E-mail addresses: suo-yang@umn.edu (S. Yang), vigor@gatech.edu (V. Yang).

¹ Current affiliation: Department of Mechanical Engineering, University of Minnesota - Twin Cities, Minneapolis, MN 55455, USA.

Nomenclature

A_i	Jacobian matrix of convection flux w.r.t. primitive state variables
A_i^v	Jacobian matrix of diffusion flux w.r.t. primitive state variables
\tilde{C}	Favre-filtered progress variable
d	jet diameter (m)
\tilde{E}	Favre-filtered total energy (J kg^{-1})
F_i	convection flux vector of conservative state variables in the i th direction
F_i^v	diffusion flux vector of conservative state variables in the i th direction
H_i^{SGS}	sub-grid scale energy flux in the i th direction ($\text{J m}^{-2} \text{s}^{-1}$)
\tilde{k}_{bi}	Favre-filtered backward reaction rate constant of the i th reaction
\tilde{k}_{fi}	Favre-filtered forward reaction rate constant of the i th reaction
L_k	number of reactions involving the k th species
M	Mach number
N_i	number of species involved in the i th reaction
\bar{p}_g	filtered gage pressure (Pa)
Q	state vector of conservative variables
\tilde{Q}	state vector of primitive variables
Q_i^{SGS}	sub-grid scale heat flux in the i th direction ($\text{J m}^{-2} \text{s}^{-1}$)
\tilde{q}_i	filtered heat flux in the i th direction ($\text{J m}^{-2} \text{s}^{-1}$)
\bar{p}	filtered pressure (Pa)
r	spatial coordinate on the radial direction (m)
S	source term vector of conservative equations
T	Jacobian matrix of conservative state variables w.r.t. primitive state variables
\tilde{T}	Favre-filtered temperature (K)
t	physical time (s)
$\tilde{U}_{k,j}$	Favre-filtered diffusion velocity component of the k th species on the j th direction (m s^{-1})
\tilde{u}_i	Favre-filtered velocity component in the i th direction (m s^{-1})
W_k	molecular weight of the k th species (kg mol^{-1})
x_i	spatial coordinate in the i th direction (m)
\tilde{Y}_k	Favre-filtered mass fraction of the k th species
\tilde{Z}	Favre-filtered mixture fraction
$\tilde{\alpha}$	Favre-filtered thermal diffusivity ($\text{m}^2 \text{s}^{-1}$)
$\tilde{\alpha}_C$	Favre-filtered diffusivity of progress variable ($\text{m}^2 \text{s}^{-1}$)
α_t	turbulent diffusivity ($\text{m}^2 \text{s}^{-1}$)
$\tilde{\alpha}_Z$	Favre-filtered diffusivity of mixture fraction ($\text{m}^2 \text{s}^{-1}$)
Γ	preconditioning matrix
δ_{ij}	Kronecker delta function
v_{ki}'	reactant stoichiometric coefficient of the k th species in the i th reaction
v_{ki}''	product stoichiometric coefficient of the k th species in the i th reaction
$\bar{\rho}$	filtered density ($\text{kg} \cdot \text{m}^{-3}$)
σ_i^{SGS}	sub-grid scale viscous work in the i th direction ($\text{J} \cdot \text{m}^{-2} \cdot \text{s}^{-1}$)
τ	pseudo time (s)
$\tilde{\tau}_{ij}$	Favre-filtered stress tensor (Pa)
τ_{ij}^{SGS}	sub-grid scale stress tensor (Pa)
$\Phi_{k,j}^{\text{SGS}}$	sub-grid scale species flux in the k th species on the j th direction ($\text{kg} \cdot \text{m}^{-2} \cdot \text{s}^{-1}$)

ϕ	equivalence ratio
$\tilde{\chi}_j$	Favre-filtered mole fraction of the j th species
$\tilde{\omega}_C$	filtered net mass production rate of progress variable ($\text{kg} \cdot \text{m}^{-3} \cdot \text{s}^{-1}$)
$\tilde{\omega}_k$	filtered net mass production rate of the k th species ($\text{kg} \cdot \text{m}^{-3} \cdot \text{s}^{-1}$)

from the mixture fraction to the corresponding reaction state. In order to overcome the drawbacks of the steady laminar flamelet model, the FPV model [10,11] was proposed to incorporate a transport equation to track a progress variable. This model has been developed to account to some extent for extinction, re-ignition, and unsteady mixing effects [10]. It cannot, however, handle multiple-feed streams without the use of a third parameter. Such a third parameter makes the look-up table very difficult to handle, due to large computer memory requirements and the need for time to build up the table. In addition, the higher-dimension look-up table results in a more complicated data retrieval process and coarser table grid. Both could introduce higher interpolation errors. Both the steady laminar flamelet and FPV models are low Mach number models, and they should not be used for high Mach number flows unless some necessary corrections are enforced.

To circumvent these limitations, detailed FRC models are desirable. The Lagrangian FDF model appears to be popular [12], because the Lagrangian framework does not introduce errors associated with the discretization of spatial gradients. These errors, however, can be re-introduced by interpolation between particles and grid points. Furthermore, for most Lagrangian FRC models, standard Eulerian approaches are still employed for the velocity components, and complicated coupling between the Eulerian and Lagrangian solvers is required. The coupling is critical in the feedback of chemistry into the flow solver, and “correction” methods are often required in the LES context [12]. Thus, Eulerian FRC models are simpler to implement and are easier to extend to a multi-scalar situation in any grid than models in the Lagrangian framework. The laminar chemistry model has shown accuracy similar to that of major Eulerian SGS closure models [13,14], so the laminar chemistry model is adopted in this study.

Compared to the reduced-order manifold models, detailed chemical kinetics in the FRC models are computationally prohibitive for LES applications due to the large number of species and the stiffness resulting from a broad range of chemical time scales. For this reason, conventional FRC-LES often employs oversimplified kinetics models, which may significantly increase uncertainties, especially in low-temperature ignition zones [15,16]. To resolve this issue, a regime-independent framework of a point-implicit stiff ODE solver (ODEPIM) [17,18] and a correlated dynamic adaptive chemistry (CoDAC) [19] were proposed. CoDAC generates locally reduced chemical kinetics for each spatial location and time step, and only calculates the reaction rates of active species and reactions. This framework has been comprehensively evaluated in the simulations of laminar plasma-assisted combustion [20], and in direct numerical simulations (DNS) of turbulent premixed [21] and non-premixed [22] flames. The approach provides a significant speed-up over the brute-force FRC, and allows for the use of relatively detailed kinetics models in FRC-LES with manageable computing resources.

Because of the mathematical nature of the governing equations, there are three primary categories of computational fluid dynamics (CFD) solvers: incompressible flow solvers, low Mach-number solvers, and fully compressible flow solvers. The intense heat release and subsequent gas expansion in turbulent combustion make incompressible flow solvers less appealing, especially when the coupling between heat release and acoustics becomes important,

as in combustion-instability studies. In low Mach-number solvers, density is decoupled from pressure (acoustics), which makes the solvers problematic near the instability limit or at high Mach numbers [23]. In fully compressible flow solvers, conservation equations are closely coupled at moderate or high Mach numbers, but become poorly coupled and numerically stiff at low Mach numbers. Many fluid flow problems involve a wide range of Mach numbers, and this poses a significant challenge for all three categories of solvers. To resolve this issue, a preconditioning method has been proposed [24–26] for treating compressible flows over a broad range of Mach numbers.

In the present study, for the first time, the highly efficient framework of ODEPIM and CoDAC is incorporated into a preconditioning scheme to allow for an Eulerian FRC-LES approach in a fully compressible flow CFD solver. The established FRC-LES framework is then used to investigate a low-speed partially premixed turbulent flame (Sandia Flame D [27]), as a benchmark case.

In the past, Sandia Flame D has been widely investigated using both reduced-order manifold and FRC models, mostly with low Mach-number CFD solvers [28, 29]. Among reduced-order manifold models, the steady laminar flamelet [30,31], Lagrangian flamelet [8,9,32], and FPV [33,34] models have been employed. Among FRC models, both the Lagrangian [12,35,36] and Eulerian [37,38] FDF models have been used, while other studies employed Eulerian models such as the laminar chemistry [1], EDC+PSR [2] and PaSR [3] models. Most of the above FRC studies used global kinetics mechanisms with a limited number of reactions, due to the prohibitive computational cost of finite-rate chemistry. In the present study, a more detailed chemical kinetics model is employed.

There have been only very few direct comparisons between the reduced-order manifold and FRC models for Sandia Flame D [1], and only the steady laminar flamelet model was used rather than a more advanced reduced-order manifold model such as the FPV model. There are few studies comparing FRC and FPV models but either for a spray flame [39] or for a swirl stabilized flame [40]. In the present work, results from the laminar FRC model are benchmarked against those from both the FPV model and experimental data, in terms of both computational performance and accuracy. The purpose of this work is to show the difference between FRC and FPV rather than showing the superiority of any model. For self-consistency, all LES combustion models are coupled with a fully-compressible CFD solver using a preconditioning scheme [24–26].

2. Theoretical formulation

Two turbulence/chemistry interaction models are considered here: the FRC and FPV models. The following sections describe in detail the formulation of both models.

2.1. Finite-rate chemistry model (FRC)

The FRC models are preferred to handle flows that involve variable Lewis-number mixing, ignition, extinction, emissions, fuel modulation, and multiple-mode combustion. To avoid interpolation between grids and particles in the Lagrangian framework, an Eulerian formulation is employed to track detailed species transport. The Favre-filtered conservation equations of mass, momentum, energy, and species concentrations are given as follows [41].

$$\frac{\partial \bar{\rho}}{\partial t} + \frac{\partial \bar{\rho} \tilde{u}_i}{\partial x_i} = 0 \quad (1)$$

$$\frac{\partial \bar{\rho} \tilde{u}_i}{\partial t} + \frac{\partial (\bar{\rho} \tilde{u}_i \tilde{u}_j + \bar{p} \delta_{ij})}{\partial x_j} = \frac{\partial (\tilde{\tau}_{ij} - \tau_{ij}^{sgs})}{\partial x_j} \quad (2)$$

$$\frac{\partial \bar{\rho} \tilde{E}}{\partial t} + \frac{\partial ((\bar{\rho} \tilde{E} + \bar{p}) \tilde{u}_i)}{\partial x_i} = \frac{\partial}{\partial x_i} (\bar{q}_i + \tilde{u}_j \tilde{\tau}_{ij} - Q_i^{sgs} - H_i^{sgs} + \sigma_i^{sgs}) \quad (3)$$

$$\frac{\partial \bar{\rho} \tilde{Y}_k}{\partial t} + \frac{\partial (\bar{\rho} \tilde{u}_j \tilde{Y}_k)}{\partial x_j} = \frac{\partial}{\partial x_j} (\bar{\rho} \tilde{U}_{k,j} \tilde{Y}_k - \Phi_{k,j}^{sgs}) + \bar{\omega}_k \quad (4)$$

In Eq. (2), the pressure gradient term $\partial \bar{p} \delta_{ij} / \partial x_j$ is proportional to $1/M^2$. For low Mach-number flows, this term becomes singular and creates numerical challenges, requiring a preconditioning scheme for a compressible flow solver [23,24]. The SGS terms are closed by algebraic Smagorinsky-like models [42,43] to account for the energy transfer from large to small scales. The filtered species mass production rate $\bar{\omega}_k$ is modeled by the laminar chemistry model. Past studies have shown that the accuracy of such an approach is similar to that of many other Eulerian SGS closure models [13,14]. The chemical source terms introduce a large and stiff ODE system, rendering detailed FRC calculations extremely expensive. The ODEPIM [17,18] and CoDAC [19–22] techniques are utilized to expedite the calculation of chemical source terms.

2.2. Flamelet/progress variable (FPV) model

In the FPV model [10,11], instead of solving filtered species equations, the transport equations of filtered mixture fraction and progress variable are solved.

$$\frac{\partial \bar{\rho} \tilde{Z}}{\partial t} + \frac{\partial (\bar{\rho} \tilde{u}_i \tilde{Z})}{\partial x_i} = \frac{\partial}{\partial x_i} \left(\bar{\rho} (\tilde{\alpha}_Z + \alpha_t) \frac{\partial \tilde{Z}}{\partial x_i} \right) \quad (5)$$

$$\frac{\partial \bar{\rho} \tilde{C}}{\partial t} + \frac{\partial (\bar{\rho} \tilde{u}_i \tilde{C})}{\partial x_i} = \frac{\partial}{\partial x_i} \left(\bar{\rho} (\tilde{\alpha}_C + \alpha_t) \frac{\partial \tilde{C}}{\partial x_i} \right) + \bar{\omega}_C \quad (6)$$

Although real diffusivities may be considered during FPV table generation, all FPV models assume a constant Lewis number in the calculation of diffusivities $\tilde{\alpha}_Z$ and $\tilde{\alpha}_C$ from thermal diffusivity $\tilde{\alpha}$. Differential diffusion effects are thus not taken into account. In regions of low turbulence intensity, turbulent diffusivity α_t is smaller than $\tilde{\alpha}_Z$ and $\tilde{\alpha}_C$. Differential diffusion effects become important and lead to relatively larger errors. The source term $\bar{\omega}_C$ for the filtered progress variable \tilde{C} is tabulated in the FPV library, and it is integrated explicitly by assuming that the time scale of the progress variable is larger than the numerical step size Δt , a situation which may not always hold true.

In this study, the mixture fraction Z is defined as:

$$Z = \frac{0.5(Y_H - Y_{H,coflow})/W_H + 2(Y_C - Y_{C,coflow})/W_C}{0.5(Y_{H,jet} - Y_{H,coflow})/W_H + 2(Y_{C,jet} - Y_{C,coflow})/W_C} \quad (7)$$

where the subscript ‘coflow’ represents the quantities in the coflow stream, and the subscript ‘jet’ the quantities in the main jet stream. The other quantities are sampled values from either simulation or experiment. The progress variable C is defined as:

$$C = Y_{CO} + Y_{CO_2} + Y_{H_2} + Y_{H_2O} \quad (8)$$

The FPV library differs from the steady laminar flamelet library in the following. First, the library is parametrized by a filtered progress variable instead of a filtered dissipation rate of mixture fraction. The library needs to cover part of the unstable branch of the S-shaped curve of ignition and extinction to account for unsteady effects. During the simulation, the filtered mass fractions and their partial derivatives for the preconditioning scheme [24–26] are retrieved from the library as functions of the filtered mixture fraction, its variance, and the filtered progress variable.

3. Numerical methods

3.1. Preconditioning scheme

The preconditioning scheme [24–26] introduces a pseudo-time derivative term to the governing equations, by pre-multiplying the primitive state vector $\hat{\mathbf{Q}}$ with a preconditioning matrix Γ :

$$\Gamma \frac{\partial \hat{\mathbf{Q}}}{\partial \tau} + \frac{\partial \mathbf{Q}}{\partial t} + \frac{\partial (\mathbf{F}_i - \mathbf{F}_i^v)}{\partial x_i} = \mathbf{S} \quad (9)$$

Here, $\hat{\mathbf{Q}}$ is defined as $\hat{\mathbf{Q}} = [\bar{p}_g \tilde{u} \tilde{v} \tilde{w} \tilde{T} | \tilde{Y}_k]^T$ to guarantee the accurate capture of acoustic waves. An implicitly iterative process is conducted for the asymptotic time advancing in the pseudo-time inner loop. When the pseudo-time iteration converges, the physical time-accurate solutions of the original governing equations are recovered. 40–60 pseudo-time iterations are typically sufficient for convergence. One advantage of the dual-time stepping integration is that instead of the stiff eigenvalues in the physical-time space, the convergence of the iterative procedure depends on the adjustable eigenvalues in the pseudo-time space. For this reason, if Γ is suitably chosen such that the eigenvalues of the Jacobian matrices in each direction are of the same order of magnitude, the resulting equations have well-conditioned eigenvalues and thus converge efficiently at all Mach numbers. The efficiency and robustness of the preconditioning method largely depend on the selection of Γ .

The dual-time advancing process consists of central differencing with artificial dissipation in space, an implicit iteration for pseudo-time integration, and an explicit fourth-order Runge–Kutta (RK4) method for physical-time integration. Specific choices for both implicit and explicit solvers are determined by the target order of time accuracy. Due to the unconditional stability of implicit solvers, the dual-time advancing process provides flexibility in the selection of time step sizes. In particular, the physical-time step size Δt is determined based on flow evolution. To capture the small chemical time scales of most species, Δt should be smaller than $\sim 0.5 \mu\text{s}$, so that the sub-cycling of ~ 50 pseudo-time steps could guarantee the capture of small chemical time scales of $\sim 10 \text{ ns}$. On the other hand, the pseudo-time step size $\Delta \tau$ is dictated by the numerical stability of the algorithm and can be modified to provide an optimal convergence rate for the pseudo-time iteration. A pseudo-time CFL number between 5 and 10 is chosen for most simulations.

To construct an implicit time advancing scheme, the preconditioned equations need to be linearized. The Jacobian matrices used in the linearization are listed as follows:

$$\mathbf{T} = \frac{\partial \mathbf{Q}}{\partial \hat{\mathbf{Q}}}, \quad \mathbf{A}_i = \frac{\partial \mathbf{F}_i}{\partial \hat{\mathbf{Q}}}, \quad \mathbf{A}_i^v = \frac{\partial \mathbf{F}_i^v}{\partial \hat{\mathbf{Q}}} \quad (10)$$

The resulting linearized preconditioned equations become:

$$\left(\Gamma + a \frac{\Delta \tau}{\Delta t} \mathbf{T} \right) \frac{\partial \hat{\mathbf{Q}}}{\partial \tau} + (\mathbf{A}_i - \mathbf{A}_i^v) \frac{\partial \hat{\mathbf{Q}}}{\partial x_i} = \mathbf{S} \quad (11)$$

To solve the equation, matrix inversion is required, and gives

$$\frac{\partial \hat{\mathbf{Q}}}{\partial \tau} + \left(\Gamma + a \frac{\Delta \tau}{\Delta t} \mathbf{T} \right)^{-1} (\mathbf{A}_i - \mathbf{A}_i^v) \frac{\partial \hat{\mathbf{Q}}}{\partial x_i} = \left(\Gamma + a \frac{\Delta \tau}{\Delta t} \mathbf{T} \right)^{-1} \mathbf{S} \quad (12)$$

3.2. Point-implicit stiff ode solver (ODEPIM)

ODEPIM [17,18] is an efficient semi-implicit stiff ODE solver. It employs a pointwise inner iteration, such that it is more efficient than fully implicit ODE solvers. Past studies [17,18] show that its accuracy is close to that of pure implicit solvers (such as the double precision variable coefficient stiff ODE solver, DVODE), but

its efficiency is close to that of fully explicit solvers (such as the RK4 and the Euler Explicit scheme with sub-cycling), especially for detailed stiff chemical kinetics. Its numerical stability allows for Δt up to $O(100 \text{ ns})$, sufficient for DNS and high-fidelity LES. The dependence of ODEPIM on the number of species in the kinetic model is very nonlinear, because the stiffness of the kinetic model may not be completely determined by the number of species.

3.3. Correlated dynamic adaptive chemistry (CoDAC)

Dynamic adaptive chemistry (DAC) [44,45] generates a reduced kinetics mechanism for each spatial location and time step by means of the path flux analysis (PFA) algorithm [46]. Only the reaction rates of selected species and reactions are calculated, while the rest are frozen to reduce the calculation demands. To reduce the large computational overhead for the PFA mechanism reduction, a correlated version of DAC (CoDAC) [19–21] is proposed to create time-space zones with similar thermo-chemical states, and the local PFA mechanism reduction is only executed once for each zone. The performance of CoDAC is almost linear with the number of species in the kinetic model, because more species can be reduced in a large kinetic model. Particularly, when the number of species is down to around 10, any further reduction is difficult in most spatial locations and time steps, and the speed-up factor of CoDAC becomes around unity.

4. Results and discussion

The Sandia flames [27] include a series of experiments employing a piloted turbulent partially premixed methane/air flame configuration. The documentation provides detailed experimental data and the flames have been widely simulated for validation purposes [8,12,38]. Previous works [11,33] on Sandia Flame D showed good agreement between FPV model predictions and experimental data, so Sandia Flame D is employed in this study as a starting point for model comparison and validation. In this study, Sandia Flame D is simulated as a benchmark using both the FPV and FRC models. To the best of our knowledge, the present work is the first attempt to employ a fully-compressible flow solver with an Eulerian FRC model for Sandia Flame D. The Reynolds number in this case is 22,400, which is relatively low. The detailed flow conditions are presented in Table 1.

Note that the flow conditions for the Sandia flame series are low Mach number, so the FPV model is valid and a preconditioning scheme must be used for fully-compressible flow solvers. Most previous studies have employed low-Mach number CFD solvers, but the present study employs a fully-compressible flow CFD solver with a preconditioning scheme due to its wider range of applicability for any Mach number. The choice of CFD solvers may contribute to the differences between results from the present study and those of previous studies.

The computation domain spans 6 mm upstream of the nozzle exit of the inlet injector, 600 mm downstream of the exit, 36 mm in the radial direction at the inlet, and 150 mm in the radial direction at the end of the domain. There are $310 \times 130 \times 64$ grid points in the axial, radial, and azimuthal directions, respectively. Grids are clustered to resolve steep gradients near both the inner and outer shear layers. The total grid number is approximately 2.6 million. 231 AMD Abu Dhabi processors are employed to perform parallel computing via the Message Passing Interface (MPI) system. The measured velocity profile and specified turbulence intensity are enforced at the inlet, while the outlet flow condition is fixed at a given back pressure. A methane kinetics mechanism with 20 species and 84 reactions, globally reduced from GRI-Mech 3.0 [47] via the Global Pathway Selection (GPS) algorithm [48], is

Table 1
Flow conditions of Sandia Flame D.

	Components	Inner diameter (mm)	Outer diameter	Bulk velocity (m/s)	Temperature (K)
Fuel jet	25% CH ₄ / 75% air (by volume)	7.2	7.7 mm	49.6	294
Piloted flame	Equilibrium: CH ₄ /air mixture ($\phi = 0.77$)	7.7	18.2 mm	11.4	1880
Co-flow	Air	18.9	N/A	0.9	291

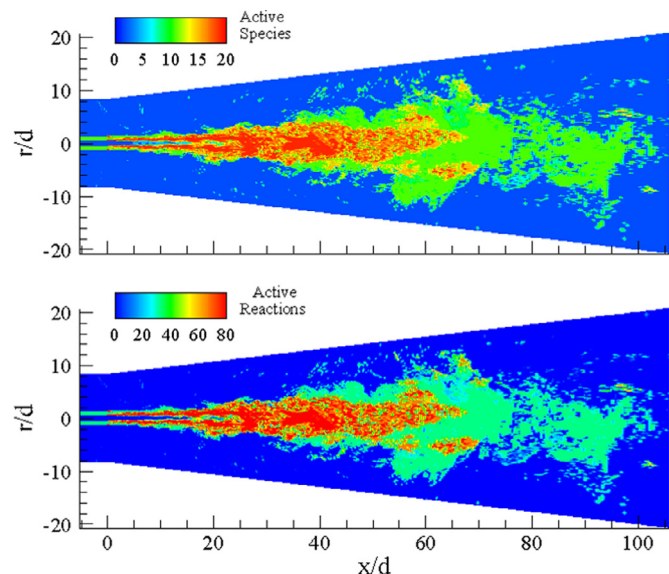


Fig. 1. Snapshots of spatial distribution of the numbers of active species (upper) and reactions (lower), generated from the CoDAC method with the FRC-LES approach.

utilized in the simulations. It has been verified in terms of homogeneous ignition delays, extinction curves in the perfectly-stirred reactor (PSR), and laminar flame speeds. The reduced methane kinetics mechanism and its verification results are provided here as supplemental materials. All time-averaged statistics are taken after three flow-through times but not longer than that, because FRC simulation is too expensive. However, the flow field has reached its statistically stationary state. The same physical time was used for both FPV and FRC to allow a fair comparison.

4.1. Computational performance

Figure 1 shows snapshots of the spatial distributions of the numbers of active species and reactions generated from the local PFA mechanism reduction (threshold=2%) of the CoDAC method. Outside the jet brush, only 2 species (preselected seed species: fuel and oxidizer) and none of the reactions are selected, because no chemical reactions occur there. In the highly-distributed turbulent partially premixed flame region, a large number of species and reactions, close to the full mechanism (20 species and 84 reactions), are selected. A large buffer zone exists between the two regions, with intermediate numbers of selected species and reactions. The reduction of the number of species and reactions in much of the spatial domain is responsible for the acceleration of the chemistry calculation from the CoDAC method. As a consequence of the highly efficient correlation technique, the PFA mechanism reduction time is more than 500 times smaller than the chemistry calculation time, and only accounts for 0.135% of the total computation time. The computational overhead of CoDAC is negligible.

Figure 2 shows the computational time of the four models. The Frozen case (multi-species transport equations without chemical kinetics source terms) serves as the theoretical upper limit for the

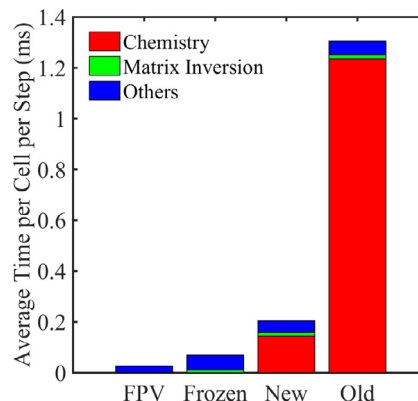


Fig. 2. Average computation time of the four models: FPV, Frozen (multi-species transport equations without chemical kinetics source terms), New (FRC model using ODEPIM and CoDAC), Old (conventional FRC model using DVODE).

computational speed of all FRC models. From the FPV to the Frozen case, the number of equations rises from 7 to 24, and the total computation time increases by a factor of 2.7, which is better than the linear computational complexity. The time for preconditioning matrix inversion increases by a factor of $11.2 \approx 3.4^2$, which is much better than the theoretical cubic computational complexity. The effective super-scaling may be due to the relatively small size of the chemical kinetics mechanism used in the present study. The chemistry calculation is expensive, and it dominates the total computation time. With respect to the conventional FRC model using DVODE, the new FRC model using ODEPIM and CoDAC significantly accelerates the chemistry calculation by a factor of 8.6, and reduces the total computation time by a factor of 6.4. Note that the performance of ODEPIM and CoDAC is limited by the unbalanced loading between different parallel processes due to the local reduction, and those processes with large number of species become the bottleneck. The chemistry time, however, still amounts to 70% of the computation time in the new FRC model, which is the largest portion of the total computation time. In contrast, preconditioning matrix inversion only accounts for 7.4% of the total computational time. The reduction of computational time in this regard is not a high priority. In summary, the computation time of the new FRC model is approximately 3 times of that of the Frozen model without chemistry, within 8 times of that of the FPV model, and 6.4 times faster than the conventional FRC model.

4.2. Spatial distribution

Figure 3 shows the time-averaged temperature distribution calculated by the FRC-LES and FPV-LES approaches. Both simulation results resemble a diffusion flame, and agree with the experimental images [27]. In the experiment, spontaneous Raman scattering of the beams from two Nd:YAG lasers (532 nm) was used to measure concentrations of the major species. The Rayleigh scattering signal was converted to temperature using a species-weighted scattering cross section, based on the Raman measurements. The flame has relatively simple flow characteristics, and the chemical reactions interlink to the local strain in both the inner and outer shear layers. Starting from approximately $x/d = 35$, an intense flame

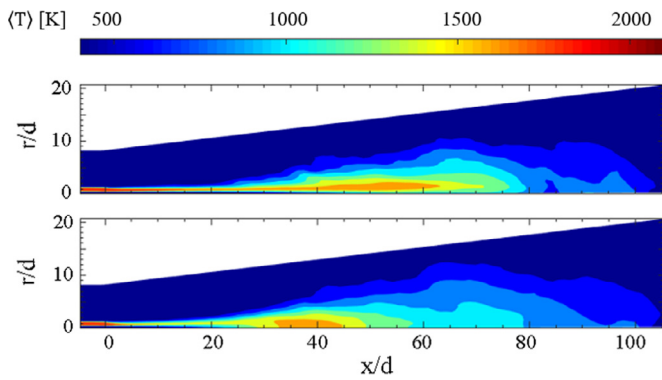


Fig. 3. Time-averaged temperature distributions from the FRC-LES (upper) and FPV-LES (lower) approaches. (For interpretation of the references to color in this figure, the reader is referred to the web version of this article.)

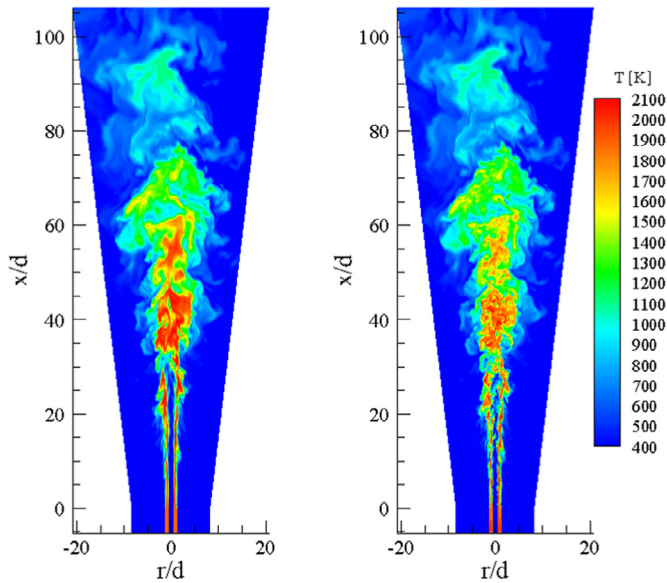


Fig. 4. Instantaneous temperature distributions from the FRC-LES (left) and FPV-LES (right) approaches at the same physical time with the same initial conditions.

region is predicted by both models, where the mixing and combustion are nearly complete and the temperature reaches approximately 1500 K or more (i.e., orange or red in Fig. 3). If the flame is defined by this region, then the flame length predicted by FRC-LES is approximately 63d, which is very close to the measured value of 67d but significantly larger than its FPV-LES counterpart of only approximately 45d.

The time-averaged results smoothen out a lot of detailed information during the temporal evolution. To reveal them, instantaneous snapshots from the two simulations using FRC and FPV models and the same initial conditions are compared at the same physical time. In contrast to the time-averaged results, the instantaneous temperature distributions from the two models show a number of distinct features, as shown in Fig. 4. The instantaneous temperature distributions from the computationally efficient FRC-LES agree well with those from the previous brute-force Eulerian FRC study by Lysenko et al. [2], and the results from the FPV-LES approach agree with those from the previous FPV study by Ihme and Pitsch [33]. It is not obvious which model leads to better agreement with the experiment observation, because of the lack of temporally resolved experimental measurements. Even though both models predict similar time-averaged statistics and spatial distributions, significant differences exist in the flame evolution, between the FRC-LES and FPV-LES approaches. The effect becomes

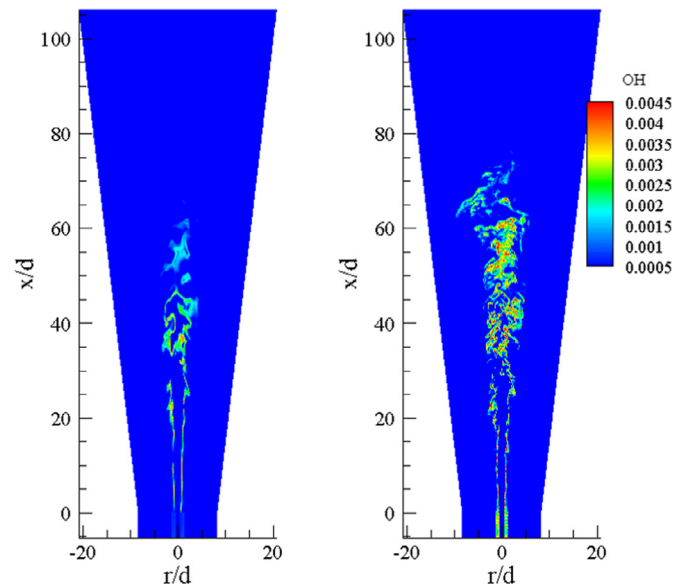


Fig. 5. Instantaneous Y_{OH} distribution from the FRC-LES (left) and FPV-LES (right) approaches at the same physical time with the same initial conditions.

profound in dealing with unsteady phenomena such as ignition, extinction, and combustion instability. This topic will be further investigated in our subsequent work on Sandia Flame E [49].

Both models predict jet flow and flame dynamics with a low level of local extinction. Near the inlet, the broad pilot flame enhances the flame stability and results in minimal local extinction. In addition, turbulence intensity is relatively low in this region, and the flow field is nearly laminar. This suggests that multi-species differential diffusion effect is important [8], a phenomenon which cannot be captured by the FPV-LES approach. In the downstream region, the outer co-flow and the inner fuel jet interact with each other in the high temperature region of the shear layer, resulting in more local extinction. In this region, the FPV-LES approach predicts significantly smaller high-temperature regions than the FRC-LES approach. Note that the large deviations between the two models is mainly in the downstream region. The FRC model is only necessary for certain combustion regimes, and the more efficient FPV model is accurate enough for the rest of Sandia Flame D.

To better understand the deviations between the two models, detailed species fields are investigated. Figure 5 compares the calculated distributions of OH radical. The FPV-LES model predicts broad distribution of OH, more regions with high OH concentration, and fewer regions with high temperature. This observation contradicts the general understanding that higher radical levels result in stronger heat release and higher temperature.

To explain this phenomenon, the distributions of CO from the two models are compared in Fig. 6. The FPV-LES model predicts both a lower peak CO level and smaller regions with high CO levels. $CO+OH=CO_2+H$ is one of the primary heat release reactions for methane flame. For this reason, CO oxidation becomes the rate-controlling step for the heat release in the FPV-LES model, which explains why this model predicts significantly smaller regions with high temperature and partially explains its over-prediction of OH. The comparison of concentrations of major products (CO_2 and H_2O) between the two models (not shown) indicates that the FPV-LES approach predicts both a lower peak product level and smaller regions with high product levels, thereby further confirming the above conclusion.

On the other hand, the FPV-LES model predicts smaller regions with high level of CH_4 (not shown). Part of the carbon element must be trapped by one of the intermediate species (mainly

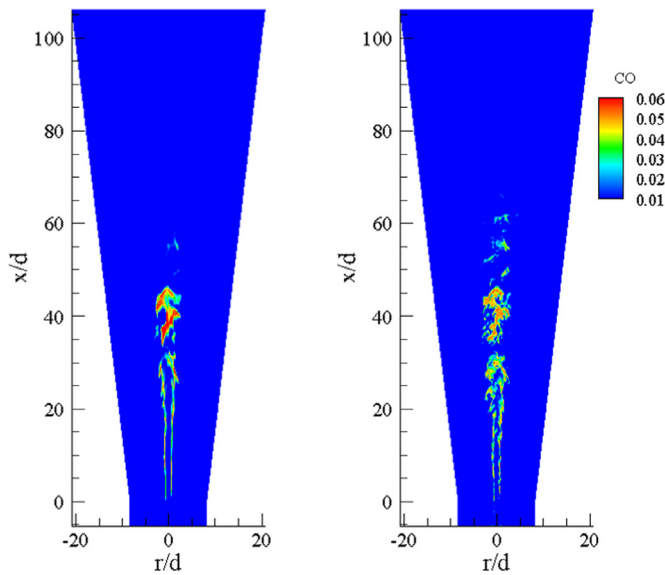


Fig. 6. Instantaneous Y_{CO} distribution from the FRC-LES (left) and FPV-LES (right) approaches at the same physical time with the same initial conditions.

CH_2O and HCO) between CH_4 and CO . The conversion from HCO to CO is very fast; only a small amount of HCO is accumulated in the flame (up to a mass fraction of 10^{-5} in the present case). In the generation of the FPV table using 1D steady counter-flow flame data, the flame temperature is higher than the actual value in turbulent combustion. The reaction $CH_2O + OH = HCO + H_2O$ tends to dominate the conversion from CH_2O to HCO . As shown in Fig. 4, however, there are many holes with a lower temperature of ~ 1200 K in an otherwise high-temperature flame zone, where $CH_2O + O_2 = HCO + HO_2$ dictates the conversion from CH_2O to HCO . In the S-curve of ignition and extinction, this intermediate-temperature region (~ 800 – 1400 K) is primarily located on the unstable middle branch. The reaction $CH_2O + O_2 = HCO + HO_2$ is thus more likely to occur during unsteady flame evolution, in which flow history information becomes important. The steady FPV table, however, cannot capture the flow history information and unsteady evolution of the flame, and has difficulty predicting the unstable branch accurately. The table could easily overlook such important reaction. As a result, in those holes, the carbon element in the FPV case is partially trapped by CH_2O and becomes difficult to convert into HCO and CO . In this problem, CH_2O is accumulated up to a mass fraction of 10^{-3} .

The deviations between the two models could come from the FPV library, the unsteady evolution of filtered mixture fraction and progress variable in the FPV-LES approach, or some combination of these two factors. For this reason, in the following sections, predictions from the two models are compared to experimental data in terms of (1) the axial and radial distributions of both mixture fraction and progress variable, and (2) the conditional statistics in the mixture fraction space.

4.3. Axial distribution of flow field

Figure 7 shows the axial profiles of time-averaged statistics for temperature and Y_{OH} (representing minor species). Similar to previous Eulerian FRC studies [2,37], the FRC-LES model under-predicts the measured mean temperature (with 3% experimental uncertainty) in the upstream region, but results in reasonably good agreement in the very downstream region. The FPV-LES result matches the upstream mean temperatures very well, but under-predicts the peak values near the intense flame region

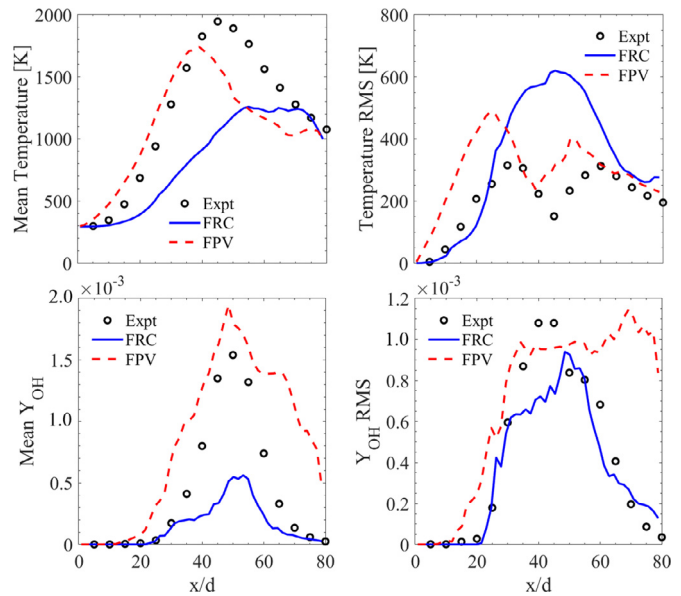


Fig. 7. Axial distributions of mean (left) and RMS (right) temperature (upper; with 3% experimental uncertainty) and Y_{OH} (lower; with 10% experimental uncertainty), from experimental measurements [27], the FRC-LES approach, and the FPV-LES approach.

($x/d = 40$ – 60) and in the downstream region. This is consistent with the observations in the snapshots of the temperature distribution (Figs. 3 and 4). In contrast, the temperatures obtained from both experiment and simulations in this study are lower than those from the reduced-order manifold models in previous studies (both the steady laminar flamelet [1] and FPV [33,34] models), possibly because earlier work employed low-Mach number CFD solvers, while the present study employs a fully-compressible flow CFD solver with a preconditioning scheme.

For normalized root-mean-square (RMS) values, the FPV-LES result matches qualitatively well with experimental data, while the FRC-LES model over-predicts the RMS data in the intense flame region possibly due to the better SGS modeling in FPV-LES. All models employed in the present and previous [1] studies over-predict the peak RMS quantities. The study by Ihme and Pitsch [33], however, slightly under-predicts the peak RMS value. It is known that RMS value is composed of fluctuations, which are sensitive and more difficult to capture than mean quantities. Comparing to temperature, a relatively larger deviation between the two models shows up for Y_{OH} (with 10% experimental uncertainty). The FRC-LES case significantly under-predicts the peak mean data, while the FPV-LES case slightly over-predicts the peak mean value, which is limited by its significant under-prediction of Y_{CO} , as discussed previously. The observation is consistent with previous FRC [37] and FPV [34] studies. The prediction of peak Y_{OH} location in the present study is more accurate than the previous Eulerian FRC study using the EDC+PSR model [2], implying that the PSR assumption is very constrained that even a simple laminar chemistry model could be more accurate than the EDC+PSR model.

Figure 8 shows the axial distributions of time-averaged statistics for mixture fraction and progress variable (representing major species). The FRC-LES model over-predicts the mean mixture fraction, while the FPV-LES model result matches well with experimental data possibly due to its better SGS modeling. Similar to previous the Eulerian FRC study by Mastata et al. [37], the FRC-LES result under-predicts the upstream mean progress variable, but matches with the very downstream values well. The FPV-LES result shows good agreement with the measured upstream mean progress variable, but under-predicts the peak value near the

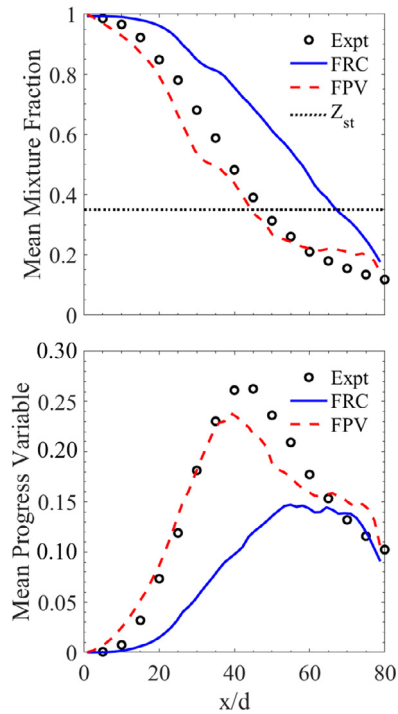


Fig. 8. Axial distributions of mean mixture fraction (upper) and progress variable (lower), from experimental measurements [27], the FRC-LES approach, and the FPV-LES approach.

intense flame region ($x/d=40-60$) and slightly over-predicts it in the very downstream region. The phenomenon is consistent with the under-prediction of temperature from the FPV model in the same intense flame region (see Figs. 3 and 4), and the FPV study by Vreman et al. [34]. In contrast, in the study by Ihme and Pitsch [33], which employed a more detailed chemical kinetics mechanism (GRI 2.11 mechanism with 49 species and 279 reactions), the FPV-LES model slightly over-predicts the mean progress variable.

In summary, the FRC-LES approach provides significantly different predictions from its FPV-LES counterpart in terms of temperature and species concentrations, and the difference is relatively larger for minor species. Note that the time evolution of the filtered progress variable significantly enhances the model prediction capability, as compared to the steady laminar flamelet model.

4.4. Radial distribution of flow field

Figure 9 shows the radial distributions of time-averaged temperature at four representative axial locations. Simulation results from both the FRC and FPV models are close to each other except near the centerline and near the peak temperature, and in roughly good agreement with experimental data (3% uncertainty) and the previous Eulerian FRC study by Mastata et al. [37]. At $x/d=7.5$, the errors of both models are smaller than those at the other three axial locations. At $x/d=15$, the FRC-LES result under-predicts the mean temperature near the centerline, while the FPV-LES result slightly under-predicts the mean temperature of the pilot flame. At $x/d=30$, FRC-LES under-predicts the mean temperature near the centerline, and show a different radial profile from the experimental data. At $x/d=45$, both models lead to under-prediction of the mean temperature near the centerline and over-prediction near the co-flow, but the FPV-LES result shows a trend consistent with experimental data.

Figure 10 shows the radial distributions of time-averaged mixture fraction at four different axial locations. The mean mixture fraction near the centerline gradually decreases along the

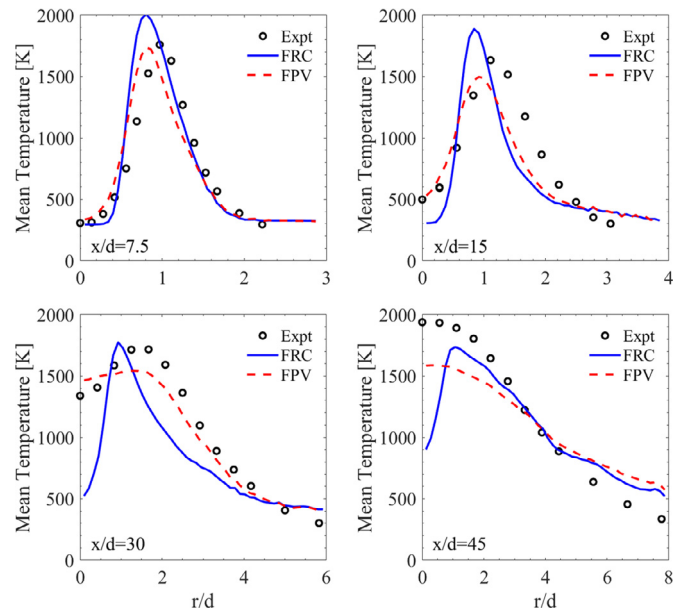


Fig. 9. Radial distributions of time-averaged temperature (with 3% experimental uncertainty) at $x/d=7.5, 15, 30, 45$, from experimental measurements [27], the FRC-LES approach, and the FPV-LES approach.

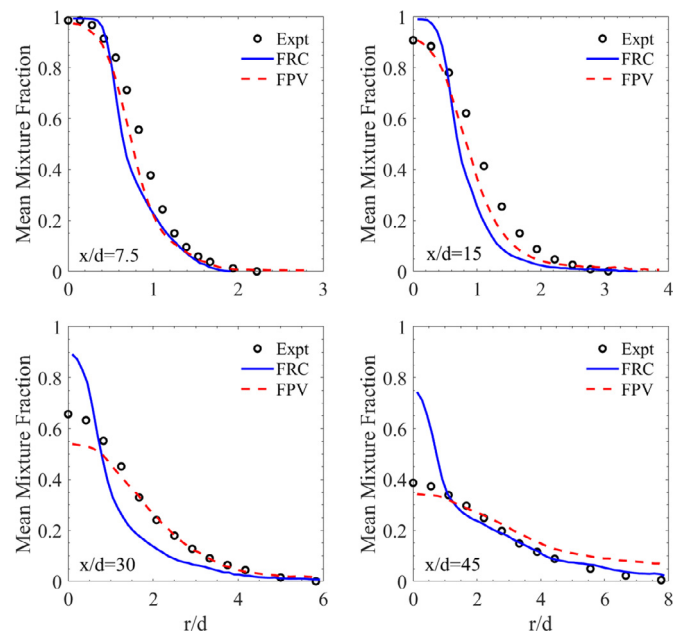


Fig. 10. Radial distributions of time-averaged mixture fraction at $x/d=7.5, 15, 30, 45$, from experimental measurements [27], the FRC-LES approach, and the FPV-LES approach.

axial direction, indicating significant breakup and consumption of the main fuel jet. At the upstream locations (i.e., $x/d=7.5, 15$), both the FRC and the FPV models give results close to each other, and show good agreement with experimental data and the Eulerian FRC study by Mastata et al. [37]. The deviation between the simulation and experimental results gradually increase along the axial direction, and FPV-LES result agrees with experimental result better than its FRC-LES counterpart possibly due to its better SGS modeling. Near the centerline, the FPV calculated mean mixture fraction agrees perfectly with the experimental data at the upstream locations (i.e., $x/d=7.5, 15$), and slightly under-predicted further downstream (at $x/d=30, 45$), possibly due to the

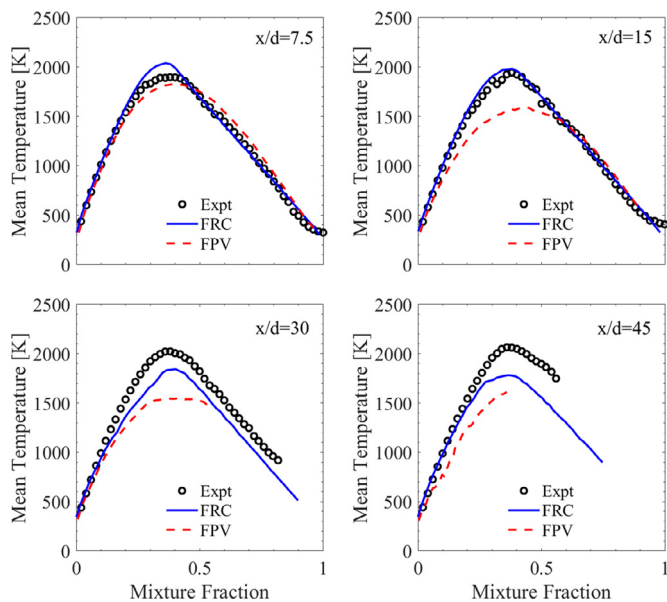


Fig. 11. Conditional average of temperature ($\langle T|Z \rangle$) (with 3% experimental uncertainty) at $x/d = 7.5, 15, 30, 45$, from experimental measurements [27], the FRC-LES approach, and the FPV-LES approach.

over-prediction of fuel jet breakup and consumption there. These trends are consistent with those in the FPV study by Vreman et al. [34]. The phenomenon of larger errors downstream may be attributed to the following reasons. First, the flame is predominantly mixing-controlled, possibly because the over-prediction of the downstream jet breakup causes an erroneous result. Second, in the simulations, the inlet velocity and turbulence are specified using experimental data, while the outlet flow condition is enforced with a fixed backpressure. For this reason, predictions in the upstream region tend to be more accurate, and errors may accumulate in the downstream region. Third, unsteady flame behaviors such as local extinction and re-ignition are challenging to capture accurately, and they occur more frequently in the downstream region than in the upstream region.

4.5. Conditional statistics

Since the two models predict similar mixture fraction profiles at the upstream locations, as discussed in the previous two sections, the deviations in temperature and species profiles can be properly represented by conditional statistics in the mixture fraction space. In addition, the conditional statistics provide deeper insight into turbulence/chemistry interactions, and can better indicate the difference between the FPV and FRC models without the influence of SGS modeling.

Figure 11 shows the conditional mean temperature at four different axial locations of $x/d = 7.5, 15, 30$, and 45 . Results from the two models contain noticeable deviations. In particular, the FRC-LES result agrees with experimental data (3% uncertainty) more closely than the FPV-LES counterpart at all locations, especially at $x/d = 15$. The predictability of the FRC-LES approach is better in the upstream region than in the downstream region. One factor contributing to this phenomenon lies in the fact that the upstream region (near the inlet) contains smaller turbulence intensity, and differential diffusion effects become important. In the upstream region ($x/d = 7.5$ and 15), the FRC-LES result agrees perfectly with experimental data for almost the entire range of mixture fraction. In the downstream region ($x/d = 30$ and 45), both models agree well with experimental data on the fuel-lean side, but under-predict the mean temperature on the fuel-rich side. In

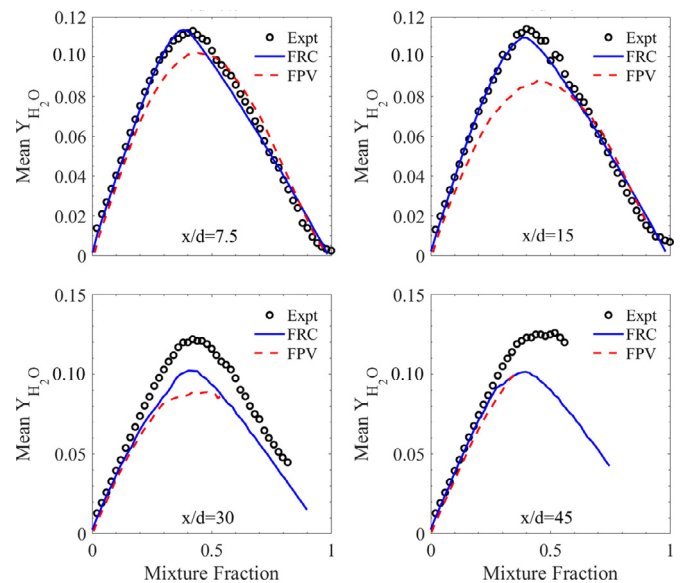


Fig. 12. Conditional average of Y_{H_2O} (i.e., $\langle Y_{H_2O}|Z \rangle$; with 4% experimental uncertainty) at $x/d = 7.5, 15, 30, 45$, from experimental measurements [27], the FRC-LES approach, and the FPV-LES approach.

contrast, the previous FPV study by Ihme and Pitsch [33] slightly over-predicts the mean temperature on the fuel-rich side, possibly due to the use of a more detailed chemical kinetics mechanism (GRI 2.11 mechanism with 49 species and 279 reactions). The present FPV model employs a smaller kinetics model to be benchmarked with the FRC model, in which a detailed kinetics model is not computationally affordable. Near the stoichiometric mixture fraction ($Z = 0.35$), comparing to the FRC-LES approach, the FPV-LES approach under-predicts the peak temperature, consistent with the comparison of the snapshots of the temperature field (Figs. 3 and 4). As a consequence of the jet breakup and fuel consumption in the downstream region, all profiles end up with mixture fraction values smaller than unity.

Figure 12 shows the conditional mean Y_{H_2O} representing major products. The calculated profiles and performance of the two models resemble those of the conditional mean temperature. The result indicates that major heat release is closely correlated with the formation of H_2O . The magnitude of Y_{H_2O} at $x/d = 45$ is higher than that at $x/d = 15$, suggesting the occurrence of re-ignition. The strong partially premixed burning (that is, the triple-flame structure) at $x/d = 45$ leads to a plateau in the Y_{H_2O} profile, as evidenced in both FRC-LES and experimental data, a situation which does not exist in diffusion flames. The FRC-LES result agrees well with experimental data (4% uncertainty), and is better than the FPV-LES counterpart in the entire domain. The FPV-LES model, however, predicts less major products than the FRC-LES model near the stoichiometric mixture fraction ($Z = 0.35$).

Figure 13 shows good agreement between the calculated and measured conditional mean Y_{CH_4} . The FRC-LES appears to be slightly more appropriate than the FPV-LES case in the upstream region; the deviation, however, becomes smaller than those in the temperature and Y_{H_2O} . At $x/d = 7.5$ and 15 , the FRC-LES result agrees perfectly with experimental data for the entire range of mixture fraction, due to its better capture of the FRC and differential diffusion effects. At $x/d = 30$ and 45 , both models over-predict the Y_{CH_4} level on the fuel-rich side, which is consistent with their under-prediction of temperature at the same location.

Figure 14 shows the conditional mean Y_{CO} noting that the CO-LIF experimental measurements suffer from 10% to 20% uncertainty [27]. At the upstream locations (i.e., $x/d = 7.5$ and 15),

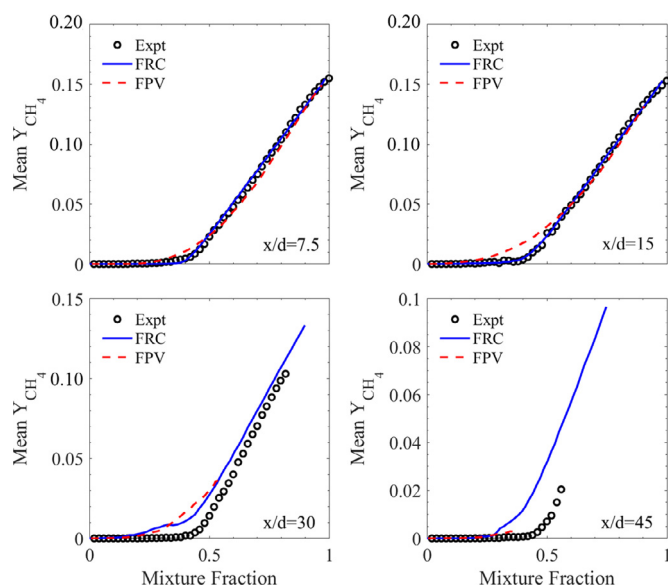


Fig. 13. Conditional average of Y_{CH_4} (i.e., $\langle Y_{CH_4}|Z \rangle$) at $x/d = 7.5, 15, 30, 45$, from experimental measurements [27], the FRC-LES approach, and the FPV-LES approach.

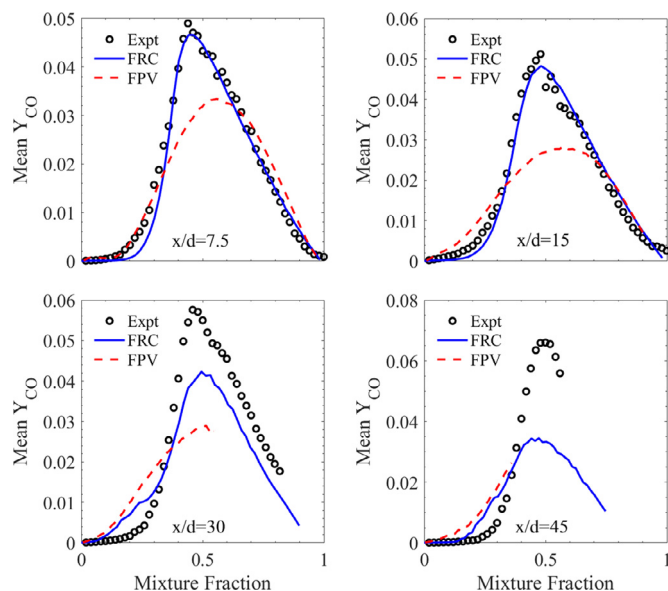


Fig. 14. Conditional average of Y_{CO} (i.e., $\langle Y_{CO}|Z \rangle$); with 10–20% experimental uncertainty) at $x/d = 7.5, 15, 30, 45$, from the CO-LIF experimental measurements [27], the FRC-LES approach, and the FPV-LES approach.

the FRC-LES result matches with the experimental data very well, while the FPV-LES result significantly under-predict the peak values. At the downstream locations (i.e., $x/d = 30$ and 45), both models show relatively small errors at highly lean or rich mixture fraction values, and under-predict the peak values near $Z = 0.5$; this explains the under-prediction of peak temperature at the same locations (Fig. 11). In contrast, previous FRC [38] and FPV [33] studies, both of which employed low-Mach number solvers, over-predict the peak values. The FRC study by Jones and Prasad [38] employed a chemical kinetics mechanism similar to the present study (a 19 species mechanism globally reduced from the GRI-Mech 3.0), so the opposite trend is likely due to different CFD solvers rather than to different chemical kinetics mechanisms. Near the inlet, the influence of the piloted flame dominates, and the peak Y_{CO} cannot directly represent the temperature peak value. As for temperature, Y_{H_2O} , and Y_{CH_4} , the FRC-LES result is

significantly better than the FPV-LES counterpart at all locations, due to its better capture of the FRC and differential diffusion effects.

5. Conclusion

An efficient finite-rate chemistry (FRC) formulation is developed and incorporated into a large eddy simulation (LES) of turbulent combustion using a preconditioned compressible flow solver. A point-implicit stiff ODE solver (ODEPIM) and a correlated dynamic adaptive chemistry (CoDAC) algorithm are employed. The CoDAC method provides effective local mechanism reduction with negligible computational overhead. As a model problem, a piloted partially premixed methane/air jet flame (Sandia Flame D), with a relatively low level of local extinction and re-ignition, is considered, and LES using both the FRC and flamelet/progress-variable (FPV) approaches are conducted. In FRC-LES, with respect to the conventional FRC model using the double precision variable coefficient stiff ODE solver (DVODE), the techniques of ODEPIM and CoDAC provide an acceleration of 8.6 times for chemistry, and 6.4 times for the total computation, using a 20-species and 84-reactions methane/air kinetics mechanism reduced from the GRI-3.0. The results of both approaches agree well with experimental measurements. The FRC-LES approach predicts larger time-averaged flame length than the FPV-LES approach, and better agrees with the measured value. This is consistent with the observation in the instantaneous flame field, where the FPV-LES approach predicts a significantly smaller high-temperature zone than the FRC-LES approach, especially in the downstream intense flame region. This is because the FPV-LES approach predicts less Y_{CO} , which becomes the rate controlling species for a primary heat release reaction $CO + OH = CO_2 + H$. For axial profiles of time-averaged statistics, the FRC-LES result is significantly different from the FPV-LES counterpart for temperature and species concentrations, and the difference is relatively larger for minor species. For radial profiles of time-averaged statistics, the two models have relatively similar predictions for temperature and mixture fraction, and agree with experimental measurements. The deviations increase along the axial direction. For both axial and radial profiles of time-averaged statistics, the FPV-LES result agrees with the experimental data better than its FRC-LES counterpart, possibly due to the better SGS modeling in FPV-LES. For conditional statistics in the mixture fraction space, the FRC-LES approach provides significantly better predictions than the FPV-LES approach for temperature and species concentrations, due to its better capture of the FRC and differential diffusion effects. The FPV-LES approach predicts lower temperature near the stoichiometric region than the FRC-LES approach, due to the bottleneck effect of CO.

Acknowledgments

This work was funded partly by the Air Force Office of Scientific Research (Grant FA9550-18-1-0216), partly by NASA (Grant NNX15AU96A), and partly by the William R.T. Oakes Endowment of the Georgia Institute of Technology.

Supplementary material

Supplementary material associated with this article can be found, in the online version, at doi:10.1016/j.combustflame.2019.08.035.

References

- [1] G. Goldin, Evaluation of LES subgrid reaction models in a lifted flame, 43rd AIAA Aerospace Sciences Meeting (2005) AIAA Paper 2005-555.

- [2] D.A. Lysenko, I.S. Ertesvåg, K.E. Rian, Numerical simulations of the Sandia flame D using the eddy dissipation concept, *Flow Turbul. Combust.* 93 (4) (2014) 665–687.
- [3] O.A. Marzouk, E.D. Huckaby, A comparative study of eight finite-rate chemistry kinetics for CO/H₂ combustion, *Eng. Appl. Comput. Fluid mech.* 4 (3) (2010) 331–356.
- [4] S. Menon, A.R. Kerstein, The linear-eddy model, *Turbulent Combustion Modeling*, Springer, Netherlands (2011), pp. 221–247.
- [5] S.B. Pope, PDF methods for turbulent reactive flows, *Prog. Energy Combust. Sci.* 11 (2) (1985) 119–192.
- [6] J.-P. Legier, T. Poinsot, D. Veynante, Dynamically thickened flame LES model for premixed and non-premixed turbulent combustion, Summer Program, Stanford, CA, Center for Turbulence Research (2000), pp. 157–168.
- [7] N. Peters, Laminar diffusion flamelet models in non-premixed turbulent combustion, *Prog. Energy Combust. Sci.* 10 (3) (1984) 319–339.
- [8] H. Pitsch, H. Steiner, Large-eddy simulation of a turbulent piloted methane/air diffusion flame (Sandia flame D), *Phys. Fluids* (1994–present) 12 (10) (2000) 2541–2554.
- [9] H. Pitsch, H. Steiner, Scalar mixing and dissipation rate in large-eddy simulations of non-premixed turbulent combustion, *Proc. Combust. Inst.* 28 (1) (2000) 41–49.
- [10] C.D. Pierce, P. Moin, Progress-variable approach for large-eddy simulation of non-premixed turbulent combustion, *J. Fluid Mech.* 504 (2004) 73–97.
- [11] H. Huo, V. Yang, Large-eddy simulation of supercritical combustion: model validation against gaseous H₂-O₂ injector, *J. Propuls. Power* 33 (5) (2017) 1272–1284.
- [12] V. Raman, H. Pitsch, A consistent LES/filtered-density function formulation for the simulation of turbulent flames with detailed chemistry, *Proc. Combust. Inst.* 31 (2) (2007) 1711–1719.
- [13] A. Potturi, J.R. Edwards, Investigation of subgrid closure models for finite-rate scramjet combustion, 51st AIAA Aerospace Sciences Meeting (2013) AIAA Paper 2013-2461.
- [14] E. Gonzalez, A. Dasgupta, S. Arshad, M. Oevermann, Effect of the turbulence modeling in large-eddy simulations of nonpremixed flames undergoing extinction and reignition, 55th AIAA Aerospace Sciences Meeting (2017) AIAA Paper 2017-0604.
- [15] R.W. Bilger, S.B. Pope, K.N.C. Bray, J.F. Driscoll, Paradigms in turbulent combustion research, *Proc. Combust. Inst.* 30 (1) (2005) 21–42.
- [16] Y. Ju, J.K. Lefkowitz, C.B. Reuter, S.H. Won, X. Yang, S. Yang, W. Sun, Z. Jiang, Q. Chen, Plasma assisted low temperature combustion, *Plasma Chem. Plasma Process.* 36 (1) (2016) 85–105.
- [17] T.R. Bussing, E.M. Murman, Finite-volume method for the calculation of compressible chemically reacting flows, *AIAA J.* 26 (9) (1988) 1070–1078.
- [18] V.R. Katta, W.M. Roquemore, Calculation of multidimensional flames using large chemical kinetics, *AIAA J.* 46 (7) (2008) 1640–1650.
- [19] W. Sun, X. Gou, H.A. El-Asrag, Z. Chen, Y. Ju, Multi-timescale and correlated dynamic adaptive chemistry modeling of ignition and flame propagation using a real jet fuel surrogate model, *Combust. Flame* 162 (4) (2015) 1530–1539.
- [20] S. Yang, V. Yang, W. Sun, S. Nagaraja, W. Sun, Y. Ju, X. Gou, Parallel on-the-fly adaptive kinetics for non-equilibrium plasma discharges of C₂H₄/O₂/Ar mixture, 54th AIAA Aerospace Sciences Meeting (2016) AIAA Paper 2016-0195.
- [21] S. Yang, R. Ranjan, V. Yang, S. Menon, W. Sun, Parallel on-the-fly adaptive kinetics in direct numerical simulation of turbulent premixed flame, *Proc. Combust. Inst.* 36 (2) (2017) 2025–2032.
- [22] S. Yang, R. Ranjan, V. Yang, W. Sun, S. Menon, Sensitivity of predictions to chemical kinetics models in a temporally evolving turbulent non-premixed flame, *Combust. Flame* 183 (2017) 224–241.
- [23] J.-S. Shuen, K.-H. Chen, Y. Choi, A coupled implicit method for chemical non-equilibrium flows at all speeds, *J. Comput. Phys.* 106 (2) (1993) 306–318.
- [24] S.-Y. Hsieh, V. Yang, A preconditioned flux-differencing scheme for chemically reacting flows at all Mach numbers, *Int. J. Comput. Fluid Dyn.* 8 (1) (1997) 31–49.
- [25] H. Meng, V. Yang, A unified treatment of general fluid thermodynamics and its application to a preconditioning scheme, *J. Comput. Phys.* 189 (1) (2003) 277–304.
- [26] N. Zong, V. Yang, An efficient preconditioning scheme for real-fluid mixtures using primitive pressure–temperature variables, *Int. J. Comput. Fluid Dyn.* 21 (5–6) (2007) 217–230.
- [27] R.S. Barlow, J.H. Frank, Effects of turbulence on species mass fractions in methane/air jet flames, *Symp. (Int.) Combust.* 27 (1) (1998) 1087–1095.
- [28] O. Desjardins, G. Blanquart, G. Balarac, H. Pitsch, High order conservative finite difference scheme for variable density low Mach number turbulent flows, *J. Comput. Phys.* 227 (15) (2008) 7125–7159.
- [29] M. Hassanaly, H. Koo, C.F. Lietz, S.T. Chong, V. Raman, A minimally-dissipative low-Mach number solver for complex reacting flows in Openfoam, *Comput. Fluids* 162 (2018) 11–25.
- [30] S. Ferraris, J.X. Wen, LES of the Sandia flame D using laminar flamelet decomposition for conditional source-term estimation, *Flow Turbul. Combust.* 81 (4) (2008) 609–639.
- [31] M.E. Mueller, G. Iaccarino, H. Pitsch, Chemical kinetic uncertainty quantification for large eddy simulation of turbulent nonpremixed combustion, *Proc. Combust. Inst.* 34 (1) (2013) 1299–1306.
- [32] X. Xu, Y. Chen, H. Wang, Detailed numerical simulation of thermal radiation influence in Sandia flame D, *Int. J. Heat Mass Transf.* 49 (13) (2006) 2347–2355.
- [33] M. Ihme, H. Pitsch, Prediction of extinction and reignition in nonpremixed turbulent flames using a flamelet/progress variable model: 2. Application in LES of Sandia flames D and E, *Combust. Flame* 155 (1) (2008) 90–107.
- [34] A. Vreman, B. Albrecht, J. Van Oijen, L. De Goey, R. Bastiaans, Premixed and nonpremixed generated manifolds in large-eddy simulation of Sandia flame D and F, *Combust. Flame* 153 (3) (2008) 394–416.
- [35] M. Nik, S. Yilmaz, P. Givi, M.H. Sheikh, S. Pope, Simulation of Sandia flame D using velocity-scalar filtered density function, *AIAA J.* 48 (7) (2010) 1513–1522.
- [36] V. Hiremath, S.R. Lantz, H. Wang, S.B. Pope, Large-scale parallel simulations of turbulent combustion using combined dimension reduction and tabulation of chemistry, *Proc. Combust. Inst.* 34 (1) (2013) 205–215.
- [37] R. Mustata, L. Valiño, C. Jiménez, W. Jones, S. Bondi, A probability density function Eulerian Monte Carlo field method for large eddy simulations: application to a turbulent piloted methane/air diffusion flame (Sandia D), *Combust. Flame* 145 (1) (2006) 88–104.
- [38] W. Jones, V. Prasad, Large Eddy simulation of the Sandia flame series (D–F) using the Eulerian stochastic field method, *Combust. Flame* 157 (9) (2010) 1621–1636.
- [39] Q. Wang, T. Jaravel, M. Ihme, Assessment of spray combustion models in large-eddy simulations of a polydispersed acetone spray flame, *Proc. Combust. Inst.* 37 (3) (2019) 3335–3344.
- [40] C. Fureby, A comparative study of flamelet and finite rate chemistry LES for a swirl stabilized flame, *J. Eng. Gas Turbine Power* 134 (4) (2012) 041503.
- [41] D. Veynante, Large eddy simulations of turbulent combustion, *Turbulence and Interactions*, Springer, 2009, pp. 113–138.
- [42] J. Smagorinsky, General circulation experiments with the primitive equations: I. the basic experiment, *Mon. Weather Rev.* 91 (3) (1963) 99–164.
- [43] P. Moin, K. Squires, W. Cabot, S. Lee, A dynamic subgrid-scale model for compressible turbulence and scalar transport, *Phys. Fluids A: Fluid Dyn.* (1989–1993) 3 (11) (1991) 2746–2757.
- [44] L. Liang, J.G. Stevens, J.T. Farrell, A dynamic adaptive chemistry scheme for reactive flow computations, *Proc. Combust. Inst.* 32 (1) (2009) 527–534.
- [45] X. Gou, Z. Chen, W. Sun, Y. Ju, A dynamic adaptive chemistry scheme with error control for combustion modeling with a large detailed mechanism, *Combust. Flame* 160 (2) (2013) 225–231.
- [46] W. Sun, Z. Chen, X. Gou, Y. Ju, A path flux analysis method for the reduction of detailed chemical kinetic mechanisms, *Combust. Flame* 157 (7) (2010) 1298–1307.
- [47] G.P. Smith, D.M. Golden, M. Frenklach, N.W. Moriarty, B. Eiteneer, M. Goldenberg, C.T. Bowman, R.K. Hanson, S. Song, W.C. Gardiner Jr., V.V. Lissianski, Z. Qin http://www.me.berkeley.edu/gri_mech/ (2016).
- [48] X. Gao, S. Yang, W. Sun, A global pathway selection algorithm for the reduction of detailed chemical kinetic mechanisms, *Combust. Flame* 167 (2016) 238–247.
- [49] S. Yang, X. Wang, V. Yang, W. Sun, Comparison of finite-rate chemistry and flamelet/progress-variable models II: Sandia flame E, 56th AIAA Aerospace Sciences Meeting (2018) AIAA Paper 2018-1427.